






Original Paper

Development and Application of a Variable-Frequency-Based Electric Sounding System for Increasing the Accuracy of Aquifer Detection

Hisafumi Asaue ¹, Katsuaki Koike ^{1,5}, Tohru Yoshinaga,² Tada-nori Goto ³,
and Hiroaki Yoshida⁴

Received 10 October 2020; accepted 11 December 2020

The demand for groundwater resources has increased owing to global developments of urbanization, industry, and agriculture. There is thus a need for advanced geophysical techniques that can be used for accurate surveying of groundwater resources. Although electric sounding has been a standard technique in surveying, it is still difficult to specify the groundwater table and aquifer distribution accurately when considering only resistivity and induced polarization. The present paper aims to improve the accuracy by developing a variable-frequency-based electric sounding system that measures apparent resistivity in the frequency range of electrical current transmittance of 1–100 Hz at intervals of 1 Hz. Experiments using soil samples and an aquifer model based on a tank show that the coefficient of variation of resistivity (C_v) in the frequency range of 21–40 Hz was effective in detecting an aquifer because it was higher than coefficients in other frequency ranges. To verify the availability of this indicator, three field experiments with different geologic settings (i.e., plateau, coastal, and limestone aquifer fields located in the southwest and on the southern edge of Japan) were undertaken. Whereas resistivity distributions varied with the current frequency depending on the field, C_v distributions were consistent regardless of the frequency common to the three test fields. Although the resistivity characteristics did not indicate the existence of a groundwater table or aquifer, C_v for the frequency range of 21–40 Hz can be used to specify the locations of the table and aquifer and additionally the doline in the limestone aquifer field. An electrokinetically induced vibration of porous material was the most plausible mechanism that explains the large C_v in the specific frequency range. The effectiveness of using C_v and the developed variable-frequency-based electric sounding system were thus demonstrated by modeling and field experiments.

KEY WORDS: Dipole–dipole electrode array, Frequency range, Resistivity, Coefficient of variation, Groundwater table.

¹Environmental Geosphere Engineering Laboratory, Department of Urban Management, Graduate School of Engineering, Kyoto University, Katsura, Kyoto, Japan.

²Technical Division, Faculty of Engineering, Kumamoto University, Kumamoto, Japan.

³Graduate School of Life Science, University of Hyogo, Himeji, Japan.

⁴Taihei Comprehensive Plan, Co., Ltd, Kumamoto, Japan.

⁵To whom correspondence should be addressed; e-mail: koike.katsuaki.5x@kyoto-u.ac.jp

INTRODUCTION

Groundwater is the largest fresh water resource for supporting life, industry, and agriculture. Global urban, industrial, and agricultural development have increased the demand for groundwater, particularly in Africa and Asia (e.g., UNESCO 2015). Methods

of geophysical prospecting that detect aquifers accurately are required to meet this demand.

Electric sounding (electrical resistivity tomography: ERT) has been the most commonly used geophysical method of detecting shallow aquifers, which are located mainly in unconsolidated deposits. Rock and soil resistivity are particularly sensitive to the water content and decreases with increasing content (Archie 1942; Fukue et al. 1999). The location, extent, and thickness of an aquifer are therefore expected to be detectable by finding a zone of relatively low resistivity in the inversion analysis of electric sounding data. For example, a broad-area image using ERT can be transformed into volumetric soil water content (Chung et al. 2019). Transient electromagnetic (TEM) survey is also an effective tool for groundwater exploration (e.g., Magaia et al. 2018). Therefore, combination of ERT and TEM survey is a good solution as demonstrated by a regional mapping of leachate distribution and possible pathways of water leakage in a tunnel construction area (Feng et al. 2020). However, the presence of clay minerals decreases the resistivity and complicates the aquifer detection solely from DC resistivity.

To discriminate water or clay as the cause of low resistivity, induced polarization (IP) methods in the time and frequency domains have been used widely. The IP effect is recognized as a macroscopic polarized charge in porous materials induced by an external electric field (e.g., Kemna et al. 2012). Its occurrence is due to electrochemical effects and polarization of the electrical double layer around grains (Marshall and Madden 1959). The physics of IP are extremely well-explained by current theories (e.g., Revil and Skold 2011; Revil et al. 2015, 2018; Abdulsamad et al. 2017). Since the early studies of electric sounding, the IP effect and model parameters of complex resistivity have been regarded useful for hydrogeologic surveys (e.g., Vacquier et al. 1957). The combination of resistivity and chargeability is thus indispensable to aquifer or water leakage detection by electric sounding (e.g., Missonou et al. 2013; Martínez-Moreno et al. 2013, 2018). A successful example is IP tomography (e.g., Abdulsamad et al. 2019), which enables imaging of both electrical conductivity and chargeability, and specifies groundwater flow path through an embankment. In addition, IP tomography can be used to image permeability (Revil and Florsch 2010), water content, and cation-exchange capacity (Revil et al. 2019).

Although research results have been accumulated and many instruments for electric sounding have been developed, the detection accuracy of aquifers and groundwater tables still remains low. Possible reasons are the limited number of frequencies for evaluation of the IP effect or the limited samplings in the time-domain decay curves of recorded field. To address the problem, this study aimed to apply ERT with a “variable frequency” system for aquifer detection. As above-mentioned, the detection accuracy of aquifers can be improved by considering the frequency dependence of the resistivity of geologic media and groundwater. A new instrument was developed in this study with usual cost of ERT instruments, scanning the resistivity structure through a number of frequencies at a band (e.g., 100 different frequencies from 1 to 100 Hz). Additionally, a method of processing resistivity data is proposed for aquifer detection. The effectiveness of the instrument and data processing method was verified in a model experiment and in three field experiments conducted in volcanic, coastal, and island areas. In this study, we employed a high-density spectrum measurement for the frequency dependence of resistivity.

INSTRUMENT DEVELOPMENT AND METHODS

An electric sounding instrument developed in this study, and called the variable-frequency-based electric sounding system (VFES), supplies an electrical current having a rectangular waveform at 1-Hz intervals in the frequency range of 1 to 100 Hz and repeatedly measures the apparent resistivity (ρ_a) of the ground at the same point. The frequency of the electric current can be changed smoothly. The VFES comprises a stabilized DC power supply, transmitter, data logger, and drive circuit for transforming a rectangular wave and a control personal computer for inputting the measurement conditions and performing measurements (Fig. 1). DC current generated by a constant-current power supply is transformed into a rectangular wave through a switching circuit. The resolution of the electric potential of the VFES is 16 bits. Features of the VFES are its high-speed sampling of sampling rate of 10,000 Hz and simultaneous measurement of ρ_a for seven underground locations.

As a traditional instrument, the VFES uses two current nodes and two potential nodes and adopts a

Development and Application of a Variable-Frequency-Based Electric Sounding System

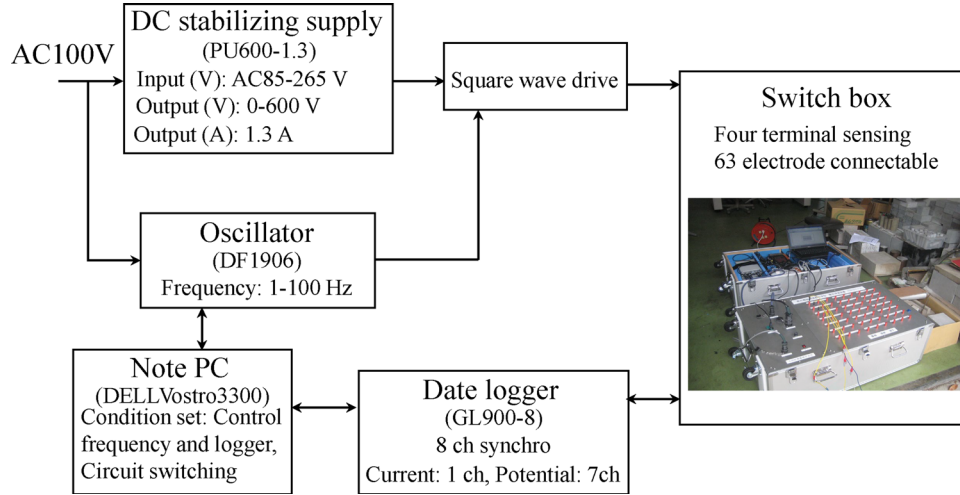


Figure 1. Configuration of the developed VFES and functional relationship among different parts.

dipole–dipole node array that has generally been used in groundwater studies to obtain a horizontally heterogeneous resistivity distribution. For this array, ρ_a is formulated as:

$$\rho_a = \frac{\pi V}{I} n(n+1)(n+2)a, \quad (1)$$

where I is the electric current (A), V is the potential difference between two nodes (V), a is the interval between two current electrodes and is the same as the interval between two potential electrodes, and n is the separation coefficient. Inversion analysis transforms ρ_a into true resistivity (ρ).

N measurements of ρ_a are expressed as an N -row matrix (\mathbf{d}), and ρ is supposed to be a row vector \mathbf{m} that has M rows; i.e., there are M true unknown resistivity data. In the inversion analysis, the difference between \mathbf{d} and ρ_a calculated using \mathbf{m} (i.e., $\Delta\mathbf{d}$) is the target of minimization using the functional, thus:

$$U = (\Delta\mathbf{d} - \mathbf{A}\Delta\mathbf{m})^T (\Delta\mathbf{d} - \mathbf{A}\Delta\mathbf{m}) + \lambda\Delta\mathbf{m}^T \Delta\mathbf{m}, \quad (2)$$

where \mathbf{A} is a Jacobean matrix with dimensions of $N \times M$, λ is a Lagrange multiplier, and $\Delta\mathbf{m}$ is the modification of the resistivity model; \mathbf{m} is repeatedly modified through iteration of the nonlinear least-squares calculation made using Eq. 2. The fitness of \mathbf{m} is evaluated in terms of the root-mean-square error (RMSE). A value of \mathbf{m} with an extremely low RMSE tends to represent an unrealistic resistivity model in which the values fluctuate largely. To avoid such over-fitting, a condition that the RMSE is

slightly less than 15% was set to select the optimum model of \mathbf{m} . We used RES2DINV (Loke et al. 2003) for the inversion analysis.

In addition to the ρ value, the coefficient of ρ variation over a certain frequency range, C_v , is defined to characterize the resistivity change with frequency:

$$C_v = \sigma/\bar{\rho}, \quad (3)$$

where σ is the standard deviation of ρ over a 20-Hz interval, and $\bar{\rho}$ is the average of ρ values in the interval. The selection of C_v and the 20-Hz interval are explained in the Discussion section.

MODEL EXPERIMENTS OF THE WATER EFFECT ON FREQUENCY-DEPENDENT RESISTIVITY

Change in Resistivity with Water and Soil Type

The first fundamental examination is to clarify the variation in resistivity with variation in frequency depending on the materials mixed with water using a sample holder. The holder is illustrated in Fig. 2. The resistivity of samples was measured using four electrodes, as in the case of the VFES. The holder and electrodes were made from acryl and platinum, respectively.

Three kinds of samples were prepared: water only, andosol mixed with water, and gravel with

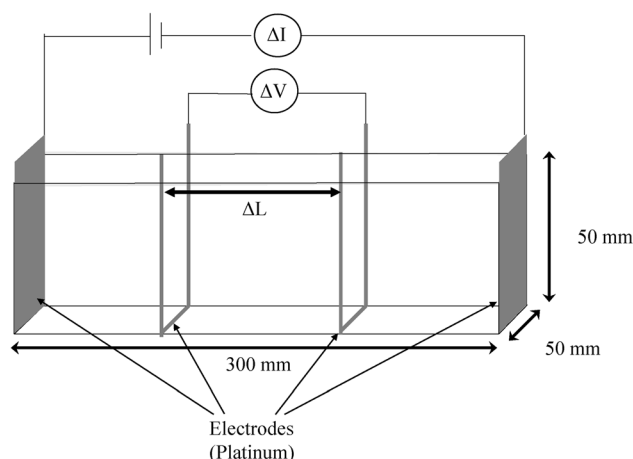


Figure 2. Layout of the apparatus for the soil-sample experiment.

water. The water only sample was taken from a spring of Lake Ezu (in Fig. 7) in Kumamoto, southwest Japan, and its electric conductivity was measured as 24 mS/m; i.e., 41 Ω m. This resistivity is within the range of the general resistivity of groundwater, 20 to 80 Ω m (Sato and Iwase 2002). Three andosol–water samples, which are each mixed with 60%, 70%, and 80% water saturation, were dried at 110 °C to clarify the effect of water content on frequency-dependent resistivity. Two gravel–water samples (i.e., saturated with water) were prepared to analyze the effect of grain size on resistivity; i.e., a sample with small grains having a diameter of 4.75 to 9.52 mm and a sample with large grains having a diameter of 19.1 mm or more.

Measurements of resistivity of the six samples are shown in Fig. 3. The resistivity of the water only sample did not change with frequency (Fig. 3a) owing to the absence of surface conduction. In contrast, the resistivities of the other five samples decreased with increasing frequency. The decreases were much larger below 40 Hz (Fig. 3b and c). Another noteworthy feature was that the oscillation of resistivity decreased with increasing water content, similar to the contact surface area between andosol and water, probably owing to the weakening effect of surface conduction. As shown in the arrows in Fig. 3b and c, the gradients of regression lines changed largely at 20 and 40 Hz common to the three (60%, 70%, and 80%) water contents of the andosol–water samples. In the case of the gravel–water samples, the resistivity increased with increasing particle

size because of decrease in water content. However, the changes in resistivity with frequency were almost parallel with each other (Fig. 3c), which may be due to there being no change in the total contact surface area between the gravel and water. An important remark is that similar to the case for andosol–water samples, there were inflection points in the gradient of the resistivity curve at 20 and 40 Hz.

Summarizing the experimental results, it is noted that the resistivity change was most distinctive in the frequency range of 1 to 40 Hz and the gradient of the resistivity curve changed most possibly owing to the condition of contact between water and particles at 20 and 40 Hz. In addition to the gradient, the oscillation of resistivity at 20 and 40 Hz is another possible cause of the large C_v values. The frequency range of 21 to 40 Hz was therefore selected as the frequency range sensitive to the existence of groundwater and applicable to aquifer detection.

Experiment Using an Aquifer Model

Based on the above experimental results for the soil–water samples, we examined the possibility of detecting the existence of groundwater using an aquifer model and resistivities in the frequency range of 21 to 40 Hz. The aquifer model was constructed from an acrylic tank of rectangular parallelepiped shape [170 cm (W : width) \times 30 cm (D : depth) \times 50 cm (H : height)], an unglazed pot

Development and Application of a Variable-Frequency-Based Electric Sounding System

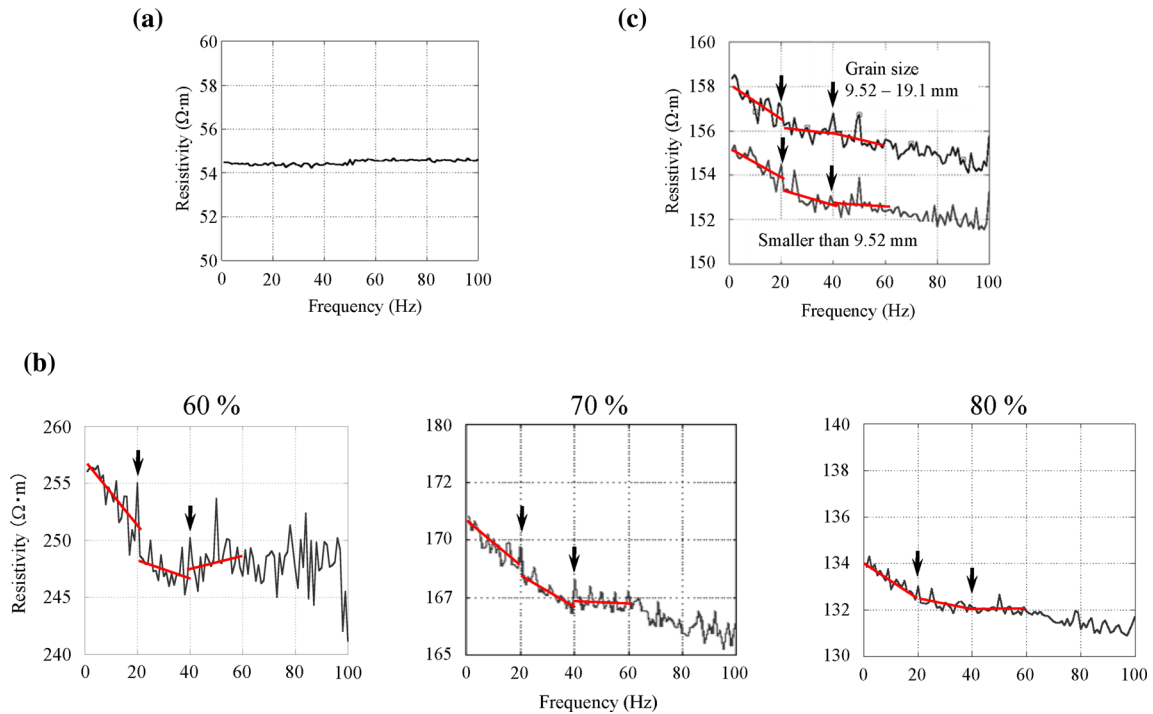


Figure 3. Resistivity change with frequency for three sample types; (a) water only sample, (b) andosol–water samples with 60%, 70%, and 80% water saturation; and (c) gravel–water samples with small grains having diameters of 4.75 to 9.52 mm and large grains having diameters of 19.1 mm or greater. Red lines in (b) and (c) indicate regression lines of the resistivity change in the 20 Hz interval, and arrows show inflection points of the gradients at 20 and 40 Hz.

[30 cm (W) \times 22 cm (D) \times 18 cm (H)] in which gravel and water were mixed to simulate an aquifer, and andosol covering the pot. To avoid disturbance of the electric field at the tank boundaries, the bottom and four side faces of the tank were covered with copper boards and grounded. In the acrylic tank, we spread andosol from the tank bottom to the 35 cm (H) and set the measurement range from 10 to 160 cm (i.e., 150 cm (W) excluding 10 cm (W) inside from the both boundaries) by the same reason. The pores of the pot were filled with water from Lake Ezu by soaking the pot in water for one day and the pot was thereafter buried at a depth of 7 cm below the surface in the middle of the tank as shown in Fig. 4. To homogenize the porosity and water content of the soil conditions, the water content of andosol was adjusted to 60% before the andosol was placed into the tank and then fully compacted. Copper electrodes were used to prevent polarization. There were 31 electrodes in total and the interval between two electrodes was set to 5 cm. Measurements with $n = 1$ to 10 were repeated three

times at each frequency to improve the data accuracy.

Taking the averages of ρ_a in four frequency ranges, namely 6–20, 21–40, 41–60, and 81–100 Hz, and performing inversion analysis, ρ distributions were obtained (Fig. 5). Here, low-frequency data from 1 to 5 Hz were not used because the noise perturbation resulted in poor quality data. In Fig. 5, the red dashed rectangle indicates the location of the pot, a simulated aquifer. Regardless of the frequency, the five ρ maps have the same general pattern of a high- ρ zone extending horizontally at mid-depth. Although there was a conspicuous gap in the continuity of the high- ρ zone in the middle of the pot, specifying the aquifer location from this feature alone was difficult.

In contrast to the above, the C_v distribution clearly varied with frequency range (Fig. 6). C_v is high in the pot area for all five frequency ranges. Among the frequency ranges, the 21 to 40 Hz range produced the highest C_v values that extended across the tank with the high anomalous values centered in

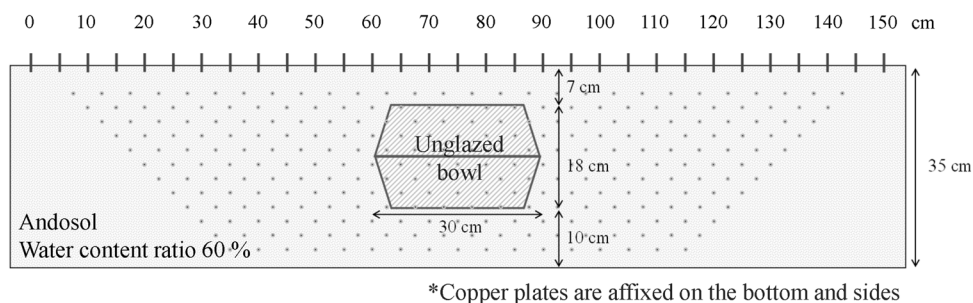


Figure 4. Layout of the apparatus for an aquifer model experiment. Copper plates are affixed on the bottom and sides.

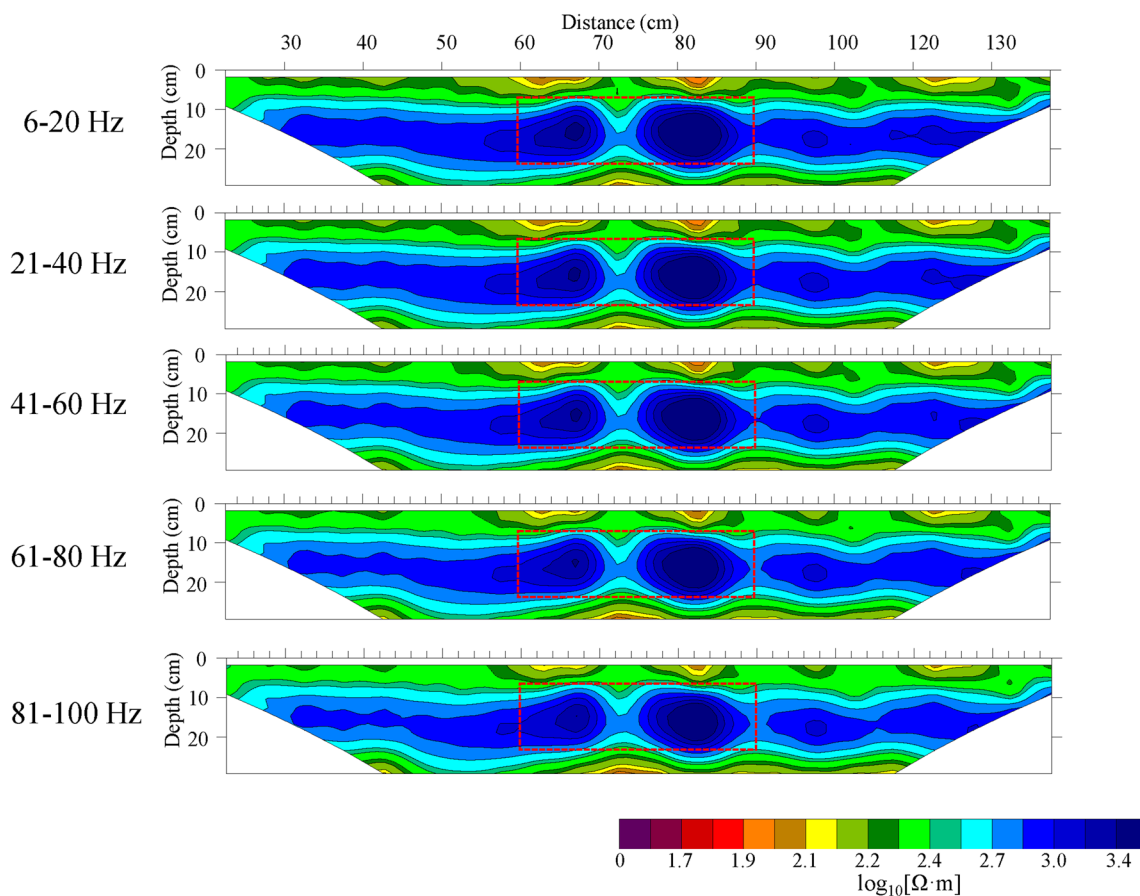


Figure 5. Resistivity distributions with different frequencies using average apparent resistivity over 15 or 20 Hz range and an inversion analysis for the aquifer model experiment. The red dashed rectangle here and in Fig. 6 indicates the location of a simulated aquifer that consists of a pot filled with gravel and water (see Fig. 4).

the area where the pot was located. The C_v anomalies outside the pot area were probably caused by local high water content of the andosol, because the water content ratio may have been

changeable despite the overall setting of 60%. C_v is thus considered to be more sensitive to the existence of groundwater and a more capable indicator than ρ itself for aquifer detection.

Development and Application of a Variable-Frequency-Based Electric Sounding System

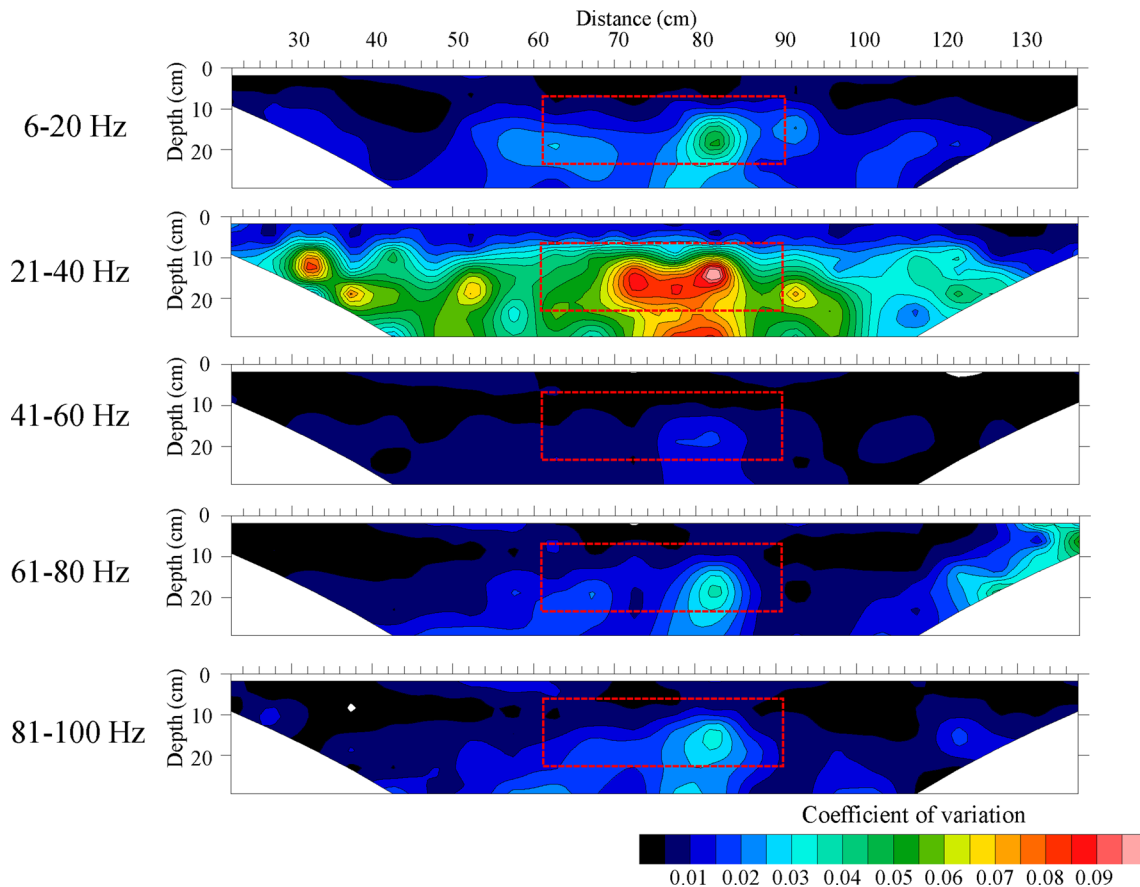


Figure 6. Distributions of the coefficient of variation obtained using resistivities at 1-Hz intervals in each frequency range for the aquifer model experiment.

FIELD EXPERIMENTS ON AQUIFER DETECTION

Results for Plateau and Coastal Fields

The effectiveness of combining V-FES and C_v was verified in two fields having different geologic settings within Kumamoto prefecture, southwest Japan; one was a lava plateau field located in the western somma of Aso Mountain and the other was a coastal field of Ariake Bay (Fig. 7a). Aquifers were confirmed to exist at shallow depths in both areas, and fresh and saline waters mix in the coastal field.

Measurements for the plateau field were conducted along a measurement or traverse line having a length of 137.5 m, a frequency range 1 to 70 Hz, $a = 5$ m, and $n = 1$ to 12 (Eq. 1). There were 258 measurement points, in total, and the maximum

survey depth was 16.4 m as computed from the a and n values, following the work of Edwards (1977). A borehole survey at the center of line found the groundwater table at a depth of 10.12 m in weathered pyroxene andesite (Shimada and Kudo 2012). This rock was covered by saprolite, reddish volcanic ash, andosol, and litter toward the surface (Fig. 7b). The location of groundwater table in the well is marked in Figs. 8 and 9.

Figure 8 shows the ρ distributions at 1, 20, and 40 Hz as examples of results. General ρ patterns on the three maps were almost the same and, common to the maps, the near-surface value of ρ was low owing to the litter and andosol soils. It was difficult to discriminate the ρ features around the groundwater table in that relatively large and small ρ values alternately appeared across the table. In terms of the C_v distributions in the three frequency ranges, 1–20, 21–40, and 41–60 Hz, a noteworthy feature was that

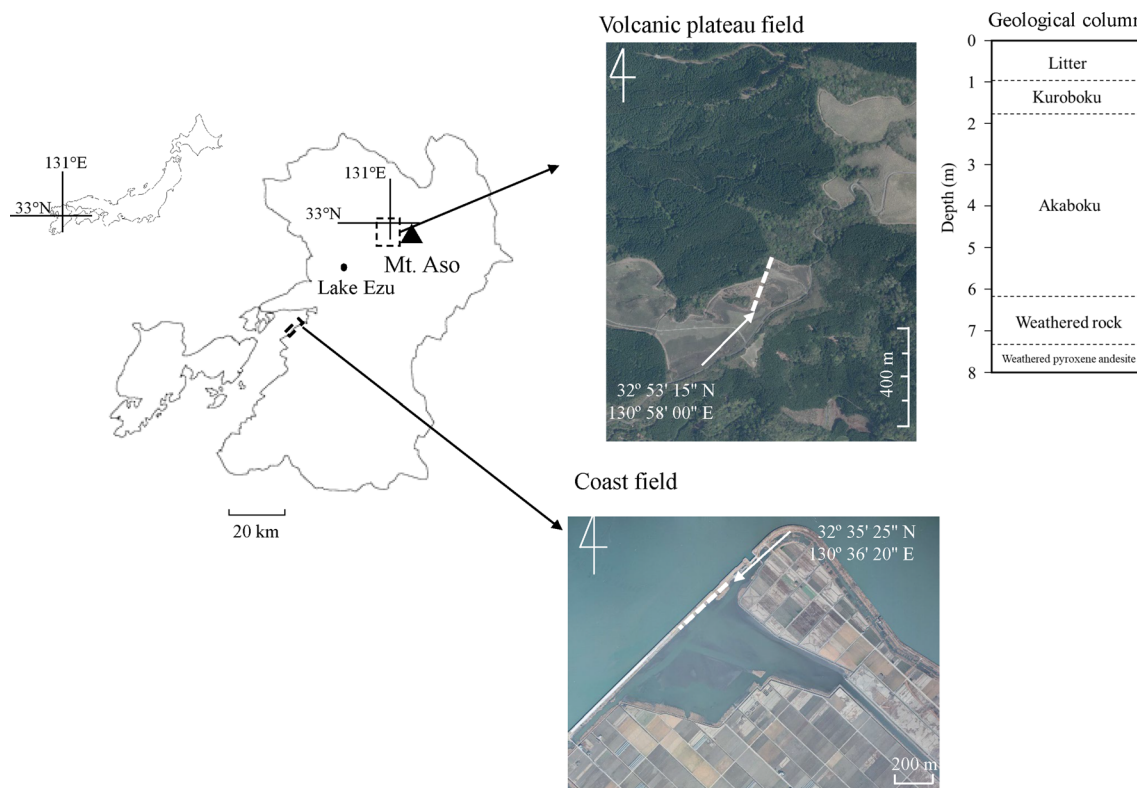


Figure 7. Selected fields for experiments and geologic columns showing main component rocks and soil types. One field is a lava plateau field located in the western somma of Aso Mountain and the other field a coastal area of Ariake Bay, both in Kumamoto prefecture, southwest Japan. Lake Ezu is a place from which water was sampled for the model experiments reported in Figs. 2, 3, 4, 5 and 6.

the largest C_v appeared around the 10 m depth, which coincided with the groundwater table in the existing borehole in the first two frequency ranges and the C_v distribution patterns were almost congruous for all frequency ranges (Fig. 9). A further detailed comparison of the two C_v maps shows that C_v values below a depth of 10 m were overall larger in the frequency range of 21 to 40 Hz. Because the aquifer in this field is known to exist in the form of a perched aquifer at this depth, this field study has demonstrated the effectiveness of the use of C_v distribution in determining the groundwater table.

The next target, the coastal field, was covered partly by concrete and had limited available locations for setting the electrode. The measurement line was therefore shorter (i.e., 30 m in length) with n limited to 5. This resulted in a total number of 90 measurement points and a maximum survey depth of 5 m. The frequency range and a were the same as for the plateau field. The groundwater table at the center of the measurement line is known to exist at a

depth of about 4 m (Taihei Comprehensive Plan 2012).

In contrast with results obtained for the plateau field, the ρ distributions differed for frequency ranges of 1, 20, and 40 Hz; i.e., the extent of the zone of low ρ within a depth of 1 m was a trend common to the three frequency ranges, but the locations of the zones having the lowest ρ were different (Fig. 10). This change in ρ with frequency may be a feature specific to groundwater mixed with saline and fresh waters. Figure 11 verifies the effectiveness of using C_v in the frequency range of 21–40 Hz in that C_v at and below the groundwater table was much greater than that for the frequency ranges of 1–20 and 41–60 Hz. Another notable merit of C_v was that the C_v patterns of the three frequency ranges were equivalent, whereas the ρ distributions varied with frequency. A table of the estimated groundwater is shown in the figure by tracing locations at which $C_v = 5.0$. The relatively high C_v values unrelated to the groundwater table, which were distributed lo-

Development and Application of a Variable-Frequency-Based Electric Sounding System

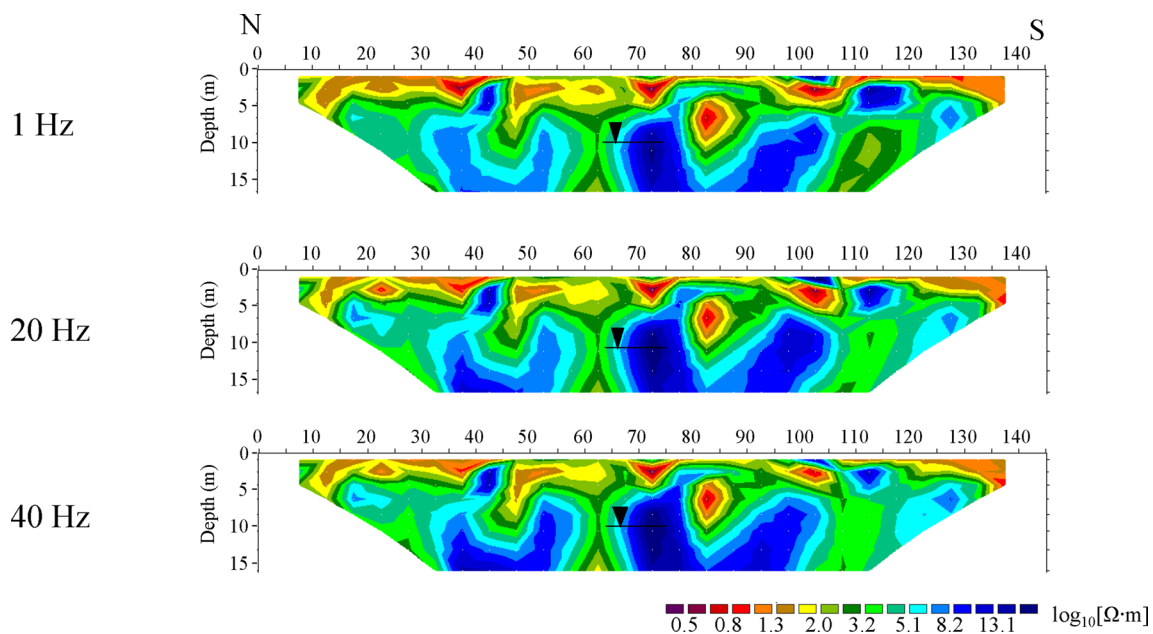


Figure 8. Resistivity distributions at 1, 20, and 40 Hz for the plateau field. The location of a drilling well and groundwater table observed in the well are overlaid here and in Fig. 9 in the form of an arrow and bar.

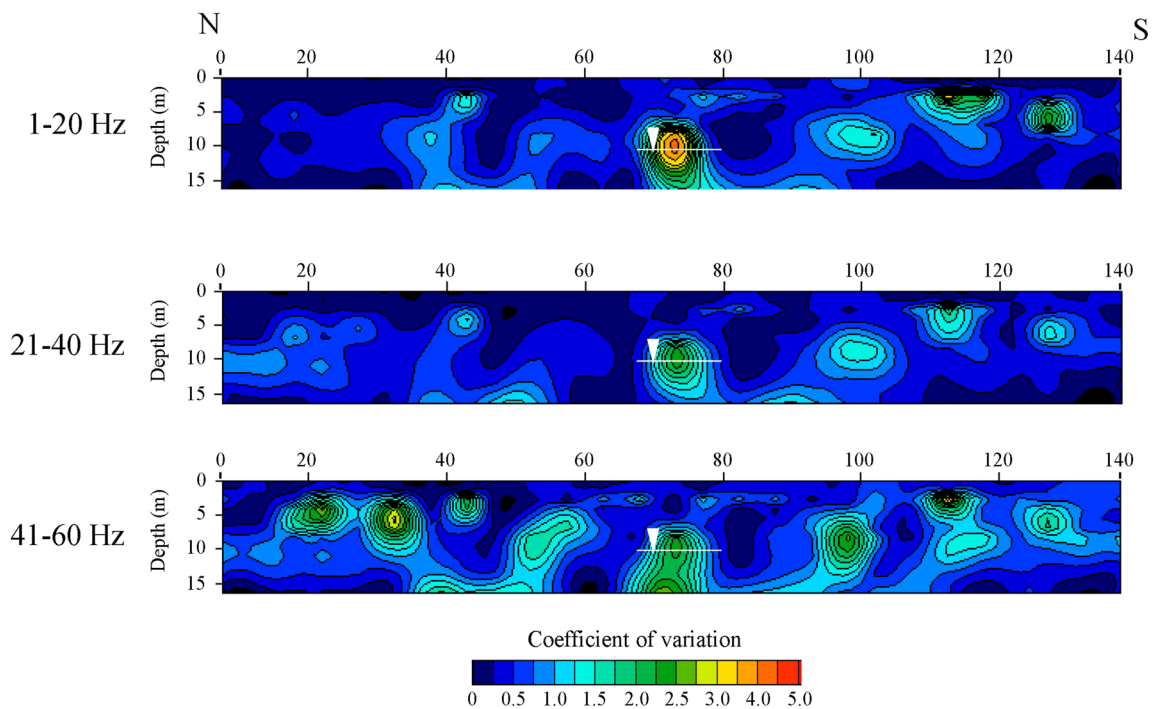


Figure 9. Distributions of the coefficient of variation in the frequency ranges of 1–20 Hz, 21–40 Hz, and 41–60 Hz for the plateau field.

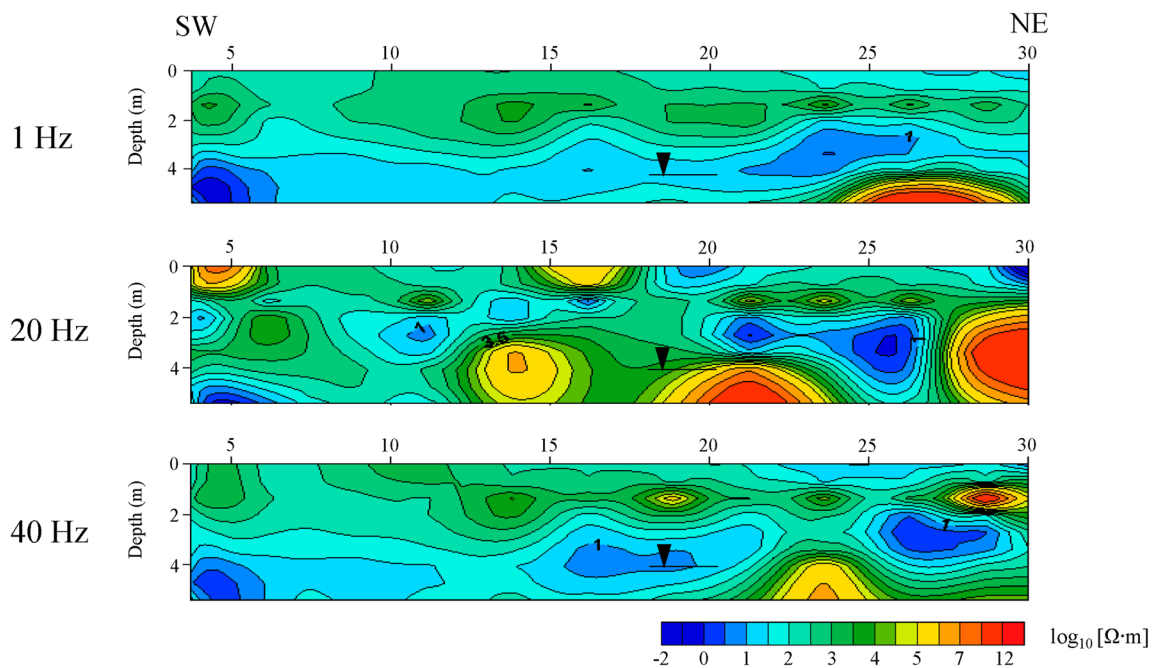


Figure 10. Resistivity distributions at 1, 20, and 40 Hz for the coastal field. The location of the drilling well and the observed groundwater table in the well are overlaid here and in Fig. 11 in the form of an arrow and bar.

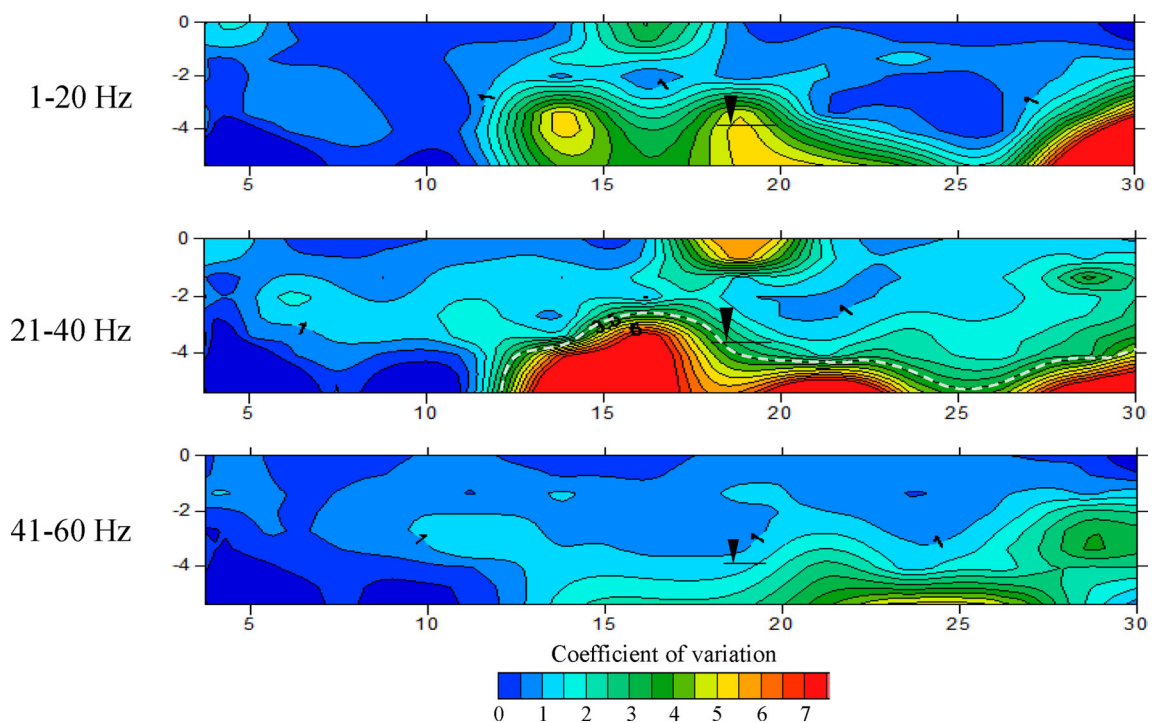


Figure 11. Distributions of the coefficient of variation in the frequency ranges of 1–20, 21–40, and 41–60 Hz for the coastal field. The dotted line shows the groundwater table estimated by tracing a large coefficient of variation (= 5.0).

Development and Application of a Variable-Frequency-Based Electric Sounding System

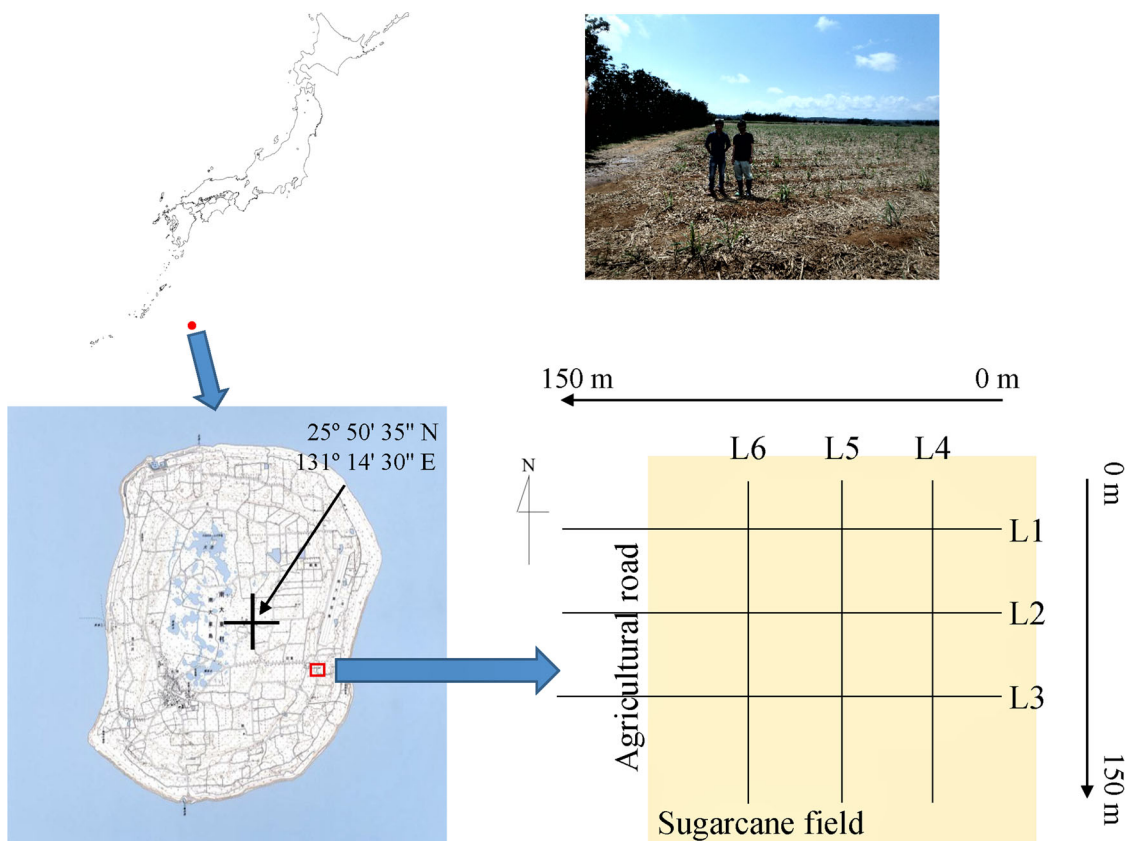


Figure 12. Selected field for a limestone aquifer containing dolines. (a) Location of Minami-Daito in the Pacific Ocean, southern edge of Japan. (b) Arrangement of six measurement lines along east-west (L1, L2, and L3) and north-south (L4, L5, and L6) directions at 35-m intervals.

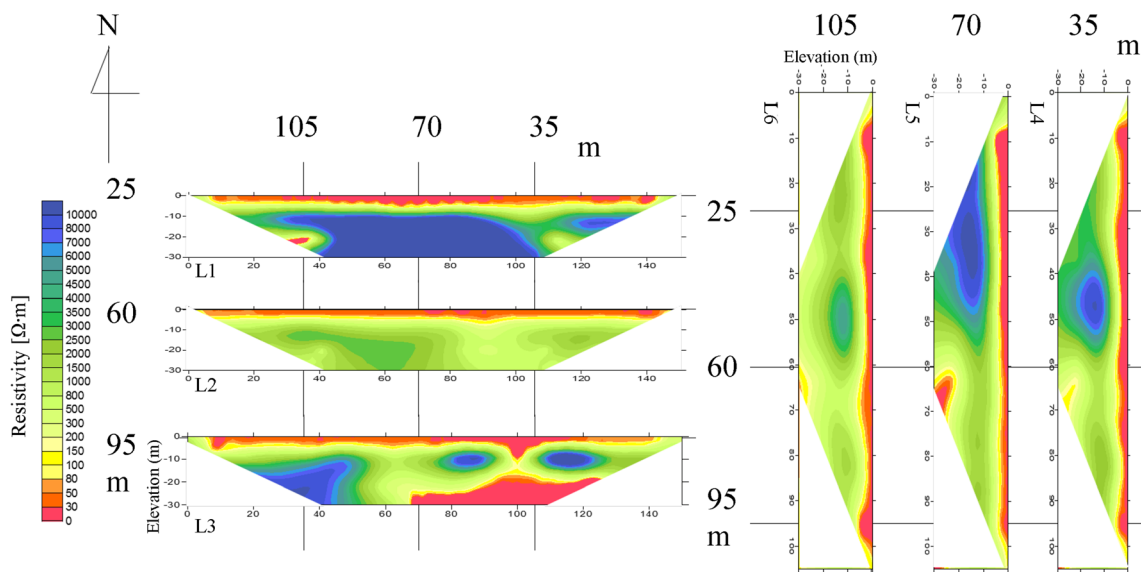


Figure 13. Resistivity distributions along the six measurement lines at 15 Hz in the limestone aquifer field.

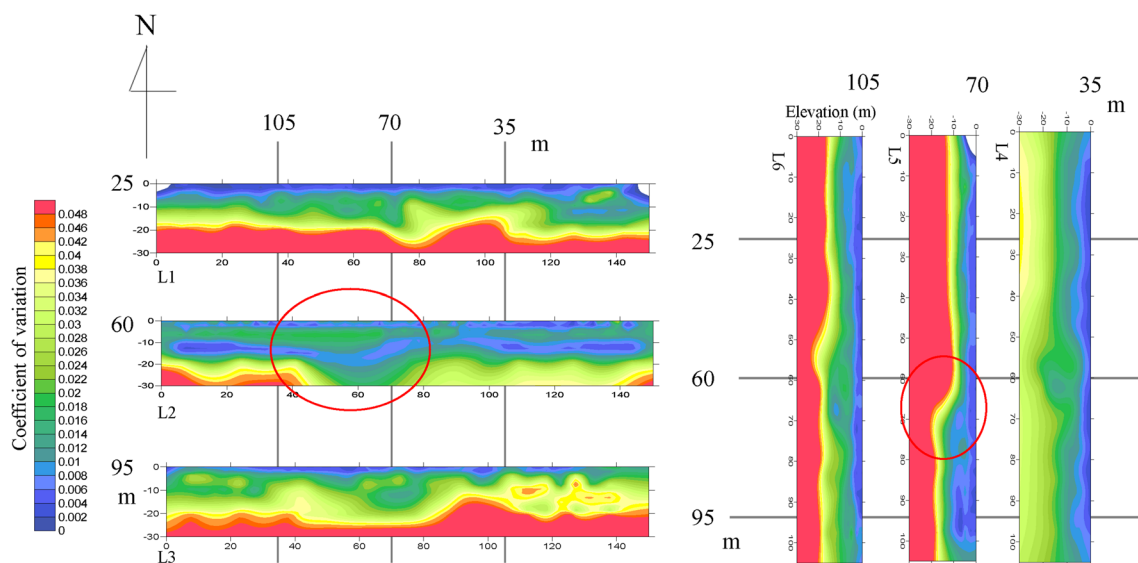


Figure 14. Distributions of the coefficient of variation in the frequency range of 1 to 20 Hz for the limestone aquifer field. A local depression of the coefficient, suggesting the formation of a doline at the intersection of Lines 2 and 5, is circled.

cally, may suggest heterogeneity of soil properties in the coastal field such as water content and salinity. In the 0 to 12 m interval, the groundwater table was thought to be located deeper because of the absence of C_v anomaly. Despite no data for interpreting this feature, a plausible possibility was existence of a buried valley there. Such valley was likely formed by the large regression in the last glacial period and the regression in Holocene in the coastal areas in Japan. The unconsolidated sediments became thick and the groundwater table can be lower in the buried valley.

Consequently, the same conclusion about the effectiveness of using C_v was drawn from the results of the two field surveys.

Result from an Island Field

A small island in the Pacific Ocean, Minami-Daito, located 340 km east of Okinawa at the southern edge of Japan and composed of limestone, was selected as a different geologic setting (Fig. 12a). The groundwater of Minami-Daito is crucial for drinking, agriculture, and industry. The middle of the island is lowland having an elevation of no more than 20 m a.s.l. and small lakes originating from submerged dolines surrounded by a plateau having an elevation of 30–50 m a.s.l. Aquifers are distributed in the form of fresh water lenses (Yang et al. 2015), and the groundwater tables are

detected in dolines and caves in many places. To clarify the spatial change in the groundwater table, three 150-m measurement lines (Lines 1, 2, and 3) and three 105-m measurement lines (Lines 4, 5, and 6) were, respectively, set along the east–west and north–south directions (Fig. 12b). Two electrode intervals, $a = 5$ and 10 m, were used along each line to reveal details of the ρ distribution over shallow to deep depths with n values up to 7. Considering the importance of the frequency range of 21–40 Hz, measurements were made for a slightly wider range, from 15 to 45 Hz.

Because the ρ distributions were almost congruous for all frequencies, a frequency of 15 Hz was selected to characterize the ρ distributions of the six lines (Fig. 13). The ρ values were different at the intersections of the two lines because of 2D measurement and inversion analysis, but the differences were 70% at most. Common to all lines, the top layers within 3 m from the ground surface were dominated by low ρ values of 50 Ω m or less, which was found by a previous study to be a feature typical of weathered limestone in the near surface (Nakazato et al. 2007). Another ρ feature was that zones of such low ρ and zones of high ρ of 5000 Ω m or more were discontinuous between adjacent lines despite the short separation of 35 m. This strong heterogeneity of ρ might originated from the local distribution of small dolines. A borehole survey found that the groundwater table near this field was at a

Development and Application of a Variable-Frequency-Based Electric Sounding System

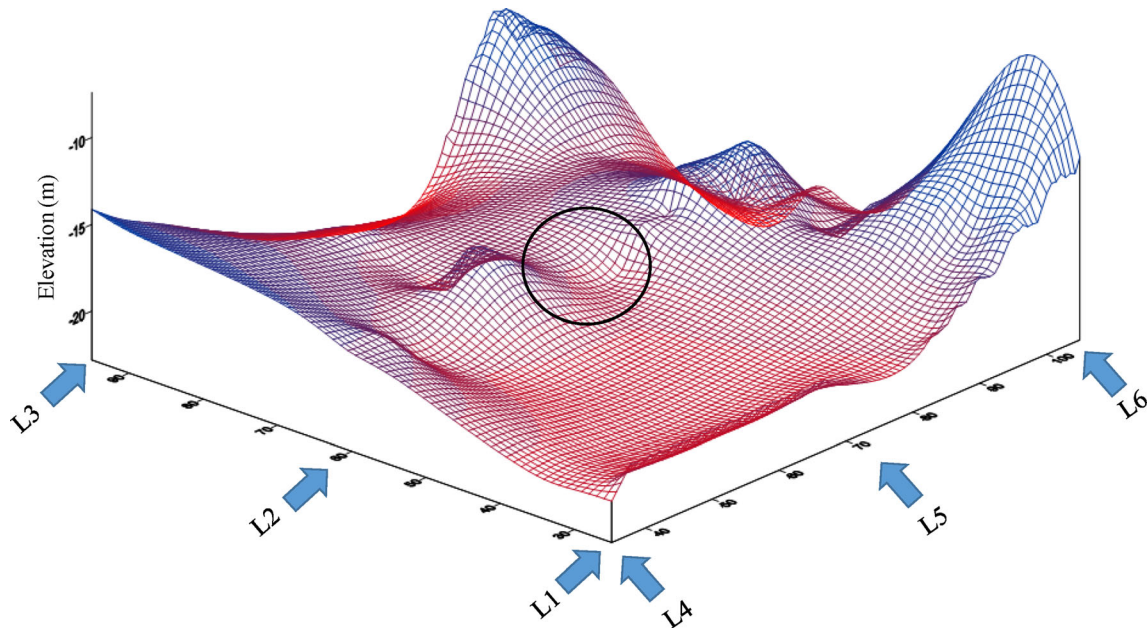


Figure 15. Perspective view of the estimated groundwater table over the limestone aquifer field obtained by tracing and interpolating locations having a coefficient of variation of 0.046 along the six lines. The location of the doline suggested in Fig. 14 is circled.

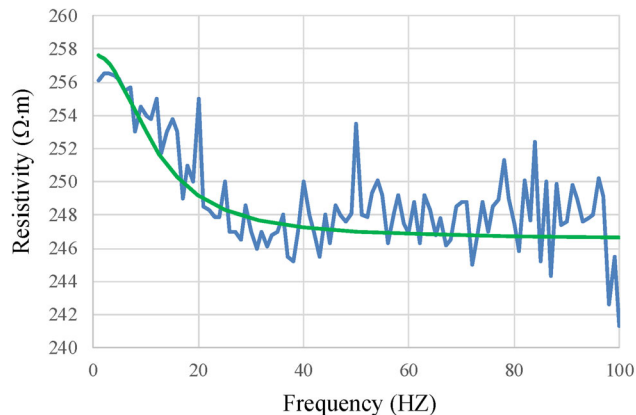


Figure 16. Fitting result of the Cole–Cole model (green curve) to the resistivity change with frequency for the andosol sample with 60% water saturation in Fig. 3b.

depth of around 15 m (Yang et al. 2015). However, as with the above two field results, the ρ characteristics did not indicate the location of the table or aquifer.

Despite the large ρ variability, the C_v distributions in the frequency range of 21 to 40 Hz were more consistent along the six lines in that C_v tended to increase with depth and deep regions were dominated by large C_v (Fig. 14). The C_v value became relatively low when the resistivity of the target area

was high. According to the information on the groundwater table mentioned above, the location of $C_v = 0.046$ can be considered as the location of the table and the aquifer may be the region of $C_v > 0.046$. The groundwater table can be estimated over the field by tracing and interpolating locations at which $C_v = 0.046$ (Fig. 15). The C_v maps also depict local depressions of the $C_v = 0.046$ location, as the intersection of Lines 2 and 5 circled in Fig. 14, which appears as a bowl shape in Fig. 15. This feature was

probably related to the formation of dolines, which were confirmed in a borehole survey conducted around the feature (Urushibara 2012). Although the above ρ characteristics suggest the effect of dolines, they did not specify the location. In addition to specifying the groundwater table and aquifer, C_v in the frequency range of 21–40 Hz can be used to specify dolines. This demonstrates the superiority of C_v and consequently the developed VFES.

DISCUSSION

The present paper investigated the physical principle of the sensitivity and effectiveness of using C_v in the frequency range of 21–40 Hz to determine the existence of groundwater. The sensitivity was obvious in the experimental results for the unglazed pot filled with water-saturated materials (Figs. 5 and 6). The frequency-dependent resistivity has been explained by the IP effect. Because this effect originates from a capacitive feature of rock or soil, frequency-domain complex resistivity models have been used to explain the effect in polarized rock formations. The Cole–Cole relaxation model (Pelton et al. 1978) is one of the well-known models:

$$\rho_e(\omega) = \rho_0 \left\{ 1 - q \left(1 - \frac{1}{1 + (i\omega\tau)^r} \right) \right\}, \quad (4)$$

where $\rho_e(\omega)$ is effective complex resistivity (Ω m) at an angular frequency $\omega = 2\pi f$; ρ_0 is DC resistivity (Ω m); τ , q , and r are, respectively, the time parameter, intrinsic chargeability, and relaxation parameter; and i is imaginary unit. Because $\rho_e(\omega)$ changes smoothly with ω , the Cole–Cole model cannot explain the fluctuation of resistivity shown in Fig. 3.

An example of Cole–Cole model fitted to the resistivity change with frequency for the andosol sample with 60% water saturation (Fig. 3b) using the Monte-Carlo method is shown in Fig. 16. One million Cole–Cole models were created randomly within parameter ranges of 200 to 300 Ω m for ρ_0 , 0 to 2 for q , τ and r , respectively, and the optimal parameter set with the minimum residual between the calculated and observed resistivity values was obtained as $\rho_0 = 258$ Ω m, $\tau = 0.0137$, $q = 0.0427$, and $r = 1.04$. The general trend of observed resistivity from 1 to 100 Hz can be represented by the optimal model (Fig. 16); however, each resistivity

peak and the large C_v feature in a narrow frequency range such as 21 to 40 Hz were never reproduced by any of the Cole–Cole models. Other modern models for the IP effect, described in “Introduction” section can produce only resistivity curves that smoothly changes with frequency. The electrochemical effect around the grains has been well-recognized as the main cause of IP effect and successfully applied to interpretations of many laboratory and field data. Nevertheless, traditional frequency-domain complex resistivity models cannot be adopted to interpret our results based on dense-frequency IP measurements. Note that the large C_v is not due to the large measurement noises, because it has a correlation with degree of the water saturation (Figs. 3 and 6).

As alternative physics, the transformation of the electric potential energy into other physical and/or chemical energies at specific frequencies is worth considering. An idea comes from the energy loss in an electrokinetic phenomenon, which may reduce the received voltages in the resistivity survey at specific frequencies. The following discussion is summarized in Fig. 17. The difference in the voltage decrease depending on the frequency range can result in a difference in the C_v magnitude with a change in the frequency range. Among the electrokinetic phenomena, electro-osmotic flow is the most plausible mechanism for the present results, because the flow, induced by an applied electric potential across a porous material, transforms electric potential energy into physical energy. In connection with the electro-osmotic flow, two equations were formulated using the electric current density \mathbf{I} (A/m^2), fluid-flow velocity \mathbf{J} (m/s), electric potential gradient $\nabla\phi$ (V/m), and pore pressure gradient ∇P (Pa/m) (Ishido and Mizuntani 1981):

$$\mathbf{I} = -L_{ee}\nabla\phi - L_{ev}\nabla P, \quad (5)$$

$$\mathbf{J} = -L_{ve}\nabla\phi - L_{vv}\nabla P, \quad (6)$$

where the first term in Eq. 5 and the second term in Eq. 6 relate, respectively, to Ohm’s law and Darcy’s law, while the second term in Eq. 5 and the first term in Eq. 6 correspond, respectively, to the streaming electric current and electro-osmotic fluid flow. L_{ee} and L_{vv} are bulk electrical conductivity and the hydraulic conductivity, respectively, and both L_{ev} and L_{ve} are electrokinetic coefficients. These phenomenological coefficients in Eqs. 5 and 6 are expressed in Ishido and Mizutani (1981) as:

Development and Application of a Variable-Frequency-Based Electric Sounding System

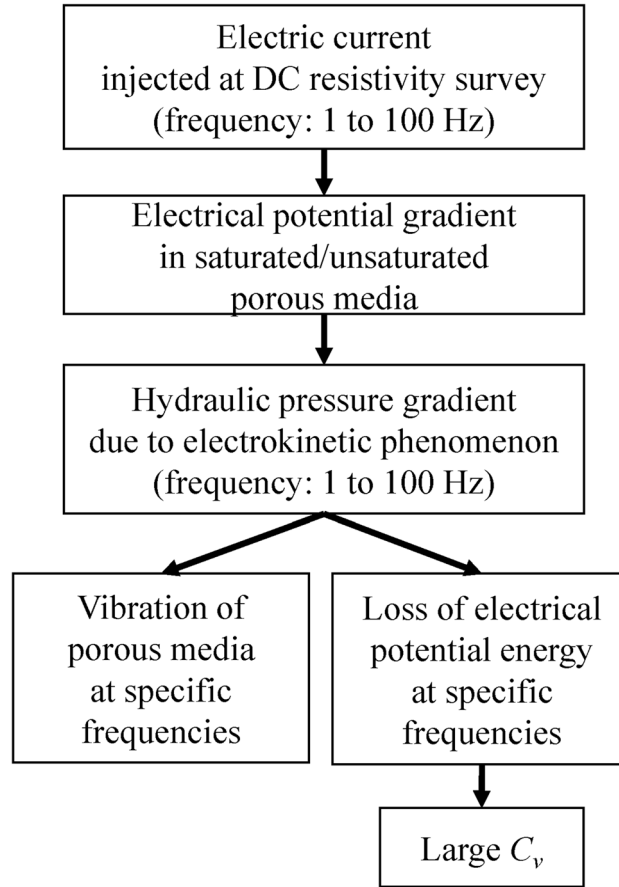


Figure 17. A flow of the most plausible mechanism for inducing large C_v in the frequency range of 21 to 40 Hz.

$$\begin{aligned}
 L_{ee} &= \phi t^{-2} \rho_f^{-1} + t^{-2} S \rho_s^{-1}, \\
 L_{vv} &= \frac{k}{\eta}, \\
 L_{ev} = L_{ve} &= -\phi t^{-2} \epsilon \zeta / \eta,
 \end{aligned} \tag{7}$$

where ρ_f and ρ_s are, respectively, the resistivity of fluid ($\Omega \text{ m}$) and the specific surface resistance (Ω); ϕ , t , S , and k are, respectively, the porosity, tortuosity, specific internal area (m^{-1}), and permeability (m^2) of the porous material; ϵ and η are, respectively, the dielectric constant (F/m) and viscosity (Pa s) of the fluid; and ζ is the zeta potential (V).

When there are no external fluid-flow sources (i.e., $\mathbf{J} = 0$), Eqs. 5, 6 and 7) give

$$\nabla P = -\frac{L_{ve}}{L_{vv}} \nabla \varphi = \frac{\phi t^{-2} \epsilon \zeta}{k} \nabla \varphi. \tag{8}$$

Supposing water and sand to be a pore-filling fluid and porous material, respectively, the parameters $\phi = 20\%$, $t = 1$, $\epsilon = 80 \times 8.9 \times 10^{-12} \text{ F/m}$, and $k = 10^{-12} \text{ m}^2$ (a value for quartz sand: Lujendijk and Gleeson 2015) and $\zeta = -17 \text{ mV}$ (Jouniaux and Ishido 2012) were assigned to calculate ∇P for the conditions of the unglazed pot experiment. The electric potential gradient $\nabla \varphi$ (V/m) can be calculated simply from the potential difference excited by the electrical current injected to the ground. Based on the theory of a DC resistivity survey (e.g., Bhattacharya 2012), the potential difference (dV_p) between two points immediately beneath two ground-surface current electrodes at a common depth (z) in earth with uniform resistivity (ρ_1) is calculated as

$$dV_p = \frac{\rho_1 I}{\pi} \left(\frac{1}{z} - \frac{1}{\sqrt{z^2 + l^2}} \right), \tag{9}$$

where l is the separation of the two current electrodes. Assuming that $\rho_1 = 1000 \Omega \text{ m}$ (as shown by the blue zone in Fig. 5), Eq. 9 gives $dV_p = 67 \text{ V}$ at $z = 10 \text{ cm}$ under the experimental conditions $l = 5 \text{ cm}$ and $I = 200 \text{ mA}$ and the average potential gradient $\nabla\phi$ ($= dV_p/l$) is therefore nearly equal to 1300 V/m . Finally, Eq. 8 was used to estimate ∇P as -33 hPa/m , corresponding to a hydraulic gradient of -33% . If such a large hydraulic gradient was generated with a frequent change in polarity (e.g., in the frequency range of 21 to 40 Hz), the AC fluctuation of hydraulic pressure probably induced vibration of the unglazed pot.

Although the frequency-dependent features of the ground-motion amplification in soils were case dependent (e.g., Bazzurro and Cornell 2004), rapid changes in amplification (i.e., peaks in the ground-motion spectrum) at several tens of Hertz have often been reported (Wen et al. 1994; Yang 2007). Therefore, the rate of transformation of electric potential energy into vibration energy can also fluctuate at several tens of Hertz. The vibration mechanism excited by electro-osmosis is complex and the loss of electric potential energy was difficult to evaluate quantitatively at present. Nevertheless, the electrokinetic vibration of porous material is the only physics that can explain the large variance of resistivity in a specific frequency range (i.e., 21–40 Hz).

The experimental results of the three fields, revealing high C_v in the frequency range of 21–40 Hz (Figs. 9, 11, and 14), can be interpreted by the above electrokinetic mechanism. For example, dV_p at a depth of 10 m was calculated as 2.7 V and $\nabla\phi$ was thus obtained as 0.54 V/m by assigning the average, ρ_1 , l , z , and I as 1000 $\Omega \text{ m}$, 5 m, 10 m, and 800 mA, respectively, for the measurement setting of the lava plateau field (Fig. 9). Because soils usually contain clays, k was modified here to a value of sand-clay mixtures with $\phi = 20\%$, 10^{-14} m^2 (Luijendijk and Gleeson 2015). Finally, ∇P at a depth of 10 m was obtained as -1.3 hPa/m , which corresponded to a hydraulic gradient of -1.3% . This gradient was comparative to or greater than values for Japanese basins and plains where groundwater is used; e.g., about 0.9% in the Kyoto Basin (Seno et al. 1963) and about 0.3% on the Kumamoto Plain (Taniguchi et al. 2003).

The electrokinetically induced vibration is likewise acceptable as a cause of the large fluctuation of resistivity under an unsaturated condition. As shown in Fig. 3b, the sample with lower water saturation had larger resistivity fluctuation. When ρ_{s-1}

is negligible, the inverse formation factor F^{-1} ($= L_{ee}/\rho f^{-1}$) is equivalent to ϕt^{-1} (Ishido and Mizutani 1981). In addition, a decrease in S_w reduces F^{-1} by a factor of S_w^v , where v is typically 2, following Archie's law (Archie 1942), and k under an unsaturated condition decreases by a factor of $S_w^{1/2} \left\{ 1 - \left(1 - S_w^{1/\theta} \right)^\theta \right\}$, where $\theta = 1 - 1/\theta_0$ and $\theta_0 = 2.03$ to 7.09 for loam soils (Van Genuchten 1980). Obviously, the condition $S_w^v > S_w^{1/2} \left\{ 1 - \left(1 - S_w^{1/\theta} \right)^\theta \right\}$ at the same S_w (< 1) was satisfied. For example, S_w^v was 0.36 and $S_w^{1/2} \left\{ 1 - \left(1 - S_w^{1/\theta} \right)^\theta \right\}$ ranged from 0.19 to 0.03 when $S_w = 0.6$, $v = 2$, and $\theta_0 = 2.03$ to 7.09. This signifies that the electric current can be kept under a low-saturation condition in which the water flow is strongly restricted. Equation 8 with a small k reveals that the lower saturation in pore spaces induces a higher pore-pressure gradient and consequently a larger vibration of soils. This phenomenon is consistent with the observed resistivity fluctuations dependent on the water saturation in Fig. 3.

CONCLUSIONS

This paper presented the development of the VFES to increase the accuracy of detecting aquifers by measuring apparent resistivity in the frequency range of 1 to 100 Hz at intervals of 1 Hz. The effectiveness of this system and the use of the variability of resistivity over a specific frequency range were demonstrated in soil–water sample and aquifer model experiments and in three field experiments with different geologic settings (i.e., plateau, coastal, and limestone aquifer fields). Note that our discoveries and conclusions were brought by the world's first system of high-density spectrum measurement, because the conventional systems use sparse frequencies. The main results obtained were summarized as follows.

- (1) In the sample experiments using andosol and gravel mixed with water, the change in resistivity was most distinct in the frequency range of 1 to 40 Hz and the oscillation of resistivity reduced with increasing water content, probably owing to the weakening effect of surface conduction.

Development and Application of a Variable-Frequency-Based Electric Sounding System

- (2) In the aquifer model experiment using an acrylic tank, an unglazed pot filled with gravel and water and andosol as filling materials, the coefficient of variation of resistivities, C_v , in the frequency range of 21 to 40 Hz was found to be the most sensitive to the existence of groundwater and a more capable indicator than resistivity for aquifer detection.
- (3) In the field experiments, resistivity distributions were almost the same over a wide frequency range for plateau and limestone aquifer fields, whereas the resistivity distribution varied with frequency for a coastal field. Nevertheless, the C_v distributions were consistent regardless of the frequency common to the three test fields. A noteworthy common feature was that although resistivity characteristics cannot be used to specify a groundwater table or aquifer, the C_v distribution in the frequency range of 21 to 40 Hz can be used to locate a table or aquifer and additionally a doline in the limestone aquifer field. The effectiveness of using C_v and the developed VFES was thus demonstrated. One of important future works was an application of VFES to detect multi-aquifers and permeable fault zone.
- (4) Electro-osmotic flow is the most plausible mechanism for the large value of C_v in the frequency range of 21 to 40 Hz. The flow induced by an applied electric potential across a porous material transforms electric potential energy into physical energy used in the AC fluctuation of hydraulic pressure, possibly resulting in the large vibration of porous soils at specific frequencies within this frequency range. This theory can also explain the phenomenon of C_v being larger under an unsaturated condition than under a saturated condition; i.e., lower saturation in pore spaces induces a higher pore-pressure gradient and consequently a larger vibration of soils.

ACKNOWLEDGMENTS

This research was conducted as a part of a Core Research for Evolutional Science and Technology

(CREST) project by Japan Science & Technology Agency (JST), entitled “Sustainable groundwater management system based on regional hydrological cycle” (research director: Jun Shimada, Professor of Kumamoto University). The authors express their gratitude to Mr. Yuji Yoshida of Kyushu Keisokki Co., Ltd. for assisting in the system design and construction, Professor Emeritus Jun Shimada of Kumamoto University for cooperating in this research and discussing the experimental results. Sincere thanks are extended to two anonymous reviewers for their valuable comments and suggestions that helped improve the clarity of the manuscript.

REFERENCES

- Abdulsamad, F., Florsch, N., & Camerlynck, C. (2017). Spectral induced polarization in a sandy medium containing semiconductor materials: Experimental results and numerical modelling of the polarization mechanism. *Near Surface Geophysics*, 15, 669–683.
- Abdulsamad, F., Revil, A., Ahmed, A. S., Coperey, A., Karaoulis, M., Nicaise, S., & Peyras, L. (2019). Induced polarization tomography applied to the detection and the monitoring of leaks in embankments. *Engineering Geology*, 254, 89–101.
- Archie, G. E. (1942). The electrical resistivity log as an aid in determining some reservoir characteristics. *Transactions of American Institute of Mining Metallurgical Engineers*, 146, 54–62.
- Bazzurro, P., & Cornell, C. A. (2004). Ground-motion amplification in nonlinear soil sites with uncertain properties. *Bulletin of the Seismological Society of America*, 94(6), 2090–2109.
- Bhattacharya, P. (2012). *Direct current geoelectric sounding: Principles and interpretation. Methods in geochemistry and geophysics* (p. 144). Amsterdam: Elsevier.
- Chung, C. C., Lin, C. P., Yang, S. H., Lin, J. Y., & Lin, C. H. (2019). Investigation of non-unique relationship between soil electrical conductivity and water content due to drying-wetting rate using TDR. *Engineering Geology*, 252, 54–64.
- Edwards, L. S. (1977). A modified pseudosection for resistivity and induced-polarization. *Geophysics*, 42, 1020–1036.
- Feng, S. J., Zhao, Y., Zhang, X. L., & Bai, Z. B. (2020). Leachate leakage investigation, assessment and engineering countermeasures for tunneling underneath a MSW landfill. *Engineering Geology*, 265, 105447.
- Fukue, M., Minato, T., Horibe, H., & Taya, N. (1999). The microstructures of clay given by resistivity measurements. *Engineering Geology*, 54, 43–53.
- Ishido, T., & Mizutani, H. (1981). Experimental and theoretical basis of electrokinetic phenomena in rock-water systems and its applications to geophysics. *Journal of Geophysical Research: Solid Earth*, 86(B3), 1763–1775.
- Jouniaux, L., & Ishido, T. (2012). Electrokinetics in earth sciences: A tutorial. *International Journal of Geophysics*, 2012, 1–16.
- Kemna, A., Binley, A., Cassiani, G., Niederleithinger, E., Revil, A., Slater, L., et al. (2012). An overview of the spectral in-

- duced polarization method for near-surface applications. *Near Surface Geophysics*, 10(6), 453–468.
- Loke, M. H., Acworth, I., & Dahlin, T. (2003). A comparison of smooth and blocky inversion methods in 2D electrical imaging surveys. *Exploration Geophysics*, 34, 182–187.
- Luijendijk, E., & Gleeson, T. (2015). How well can we predict permeability in sedimentary basins? Deriving and evaluating porosity-permeability equations for noncemented sand and clay mixtures. *Geofluids*, 15(1–2), 67–83.
- Magaia, L. A., Goto, T., Masoud, A. A., & Koike, K. (2018). Identifying groundwater potential in crystalline basement rocks using remote sensing and electromagnetic sounding techniques in central Western Mozambique. *Natural Resources Research*, 27(3), 275–298.
- Marshall, D. J., & Madden, T. R. (1959). Induced polarization: A study of its causes. *Geophysics*, 24, 658–827.
- Martínez-Moreno, F. J., Pedrera, A., Ruano, P., Galindo-Zaldívar, J., Martos-Rosillo, S., González-Castillo, L., et al. (2013). Combined microgravity, electrical resistivity tomography and induced polarization to detect deeply buried caves: Algaidilla cave (Southern Spain). *Engineering Geology*, 162, 67–78.
- Martínez-Moreno, F. J., Delgado-Ramos, F., Galindo-Zaldívar, J., Martín-Rosales, W., López-Chicano, M., & González-Castillo, L. (2018). Identification of leakage and potential areas for internal erosion combining ERT and IP techniques at the Negratín Dam left abutment (Granada, southern Spain). *Engineering Geology*, 240, 74–80.
- Misonou, T., Asaue, H., Yoshinaga, T., Matsukuma, Y., Koike, K., & Shimada, J. (2013). Hydrogeologic structure and groundwater movement imaging in a tideland zone using electrical sounding resistivity: A case study at a coastal area of the Ariake Sea, southwest Japan. *Hydrogeology Journal*, 21(7), 1593–1603.
- Nakazato, H., Kuroda, S., Inoue, K., Takeuchi, M., & Wang, Z. (2007). Visualization of tidal fluctuations on groundwater by resistivity monitoring method. *Butsuri-Tansa*, 60(6), 501–506. (in Japanese).
- Pelton, W. H., Ward, S. H., Hallof, P. G., Sill, W. R., & Nelson, P. H. (1978). Mineral discrimination and removal of inductive coupling with multifrequency IP. *Geophysics*, 43(3), 588–609.
- Revil, A., & Florsch, N. (2010). Determination of permeability from spectral induced polarization in granular media. *Geophysical Journal International*, 181(3), 1480–1498.
- Revil, A., & Skold, M. (2011). Salinity dependence of spectral induced polarization in sands and sandstones. *Geophysical Journal International*, 187, 813–824.
- Revil, A., Abdel Aal, G. Z., Atekwana, E. A., Mao, D., & Florsch, N. (2015). Induced polarization response of porous media with metallic particles-part 2: Comparison with a broad database of experimental data. *Geophysics*, 80(5), D539–D552.
- Revil, A., Coperey, A., Deng, Y., Cerepi, A., & Seleznev, N. (2018). Complex conductivity of tight sandstones. *Geophysics*, 83(2), E55–E74.
- Revil, A., Qi, Y., Ghorbani, A., Coperey, A., Ahmed, A. S., Finizola, A., & Ricci, T. (2019). Induced polarization of volcanic rocks. 3. Imaging clay cap properties in geothermal fields. *Geophysical Journal International*, 218(2), 1398–1427.
- Sato, K., & Iwasa, Y. (2002). Hydrogeology, Maruzen, p. 319. (in Japanese).
- Seno, K., Kikkawa, K., Yuhara, K., & Kawabata, H. (1963). Ground water in Kyoto city. *Special contributions of the Geophysical Institute, Kyoto University*, 3, 233–237.
- Shimada, J., & Kudo, K. (2012). Business report of consignment study of Kumamoto prefecture, 2011 f.y.: Investigation study of forest effect for groundwater recharge. p. 49. (in Japanese).
- Taihei Comprehensive Plan, Co. Ltd. (2012). Business report of consignment study of Kumamoto prefecture, 2012 f.y.: Water leak investigation for coast conservation in the Bunsei district. p. 39. (in Japanese).
- Taniguchi, M., Shimada, J., & Uemura, T. (2003). Transient effects of surface temperature and groundwater flow on subsurface temperature in Kumamoto Plain, Japan. *Physics and Chemistry of the Earth, Parts A/B/C*, 28(9–11), 477–486.
- UNESCO (2015). Water for a Sustainable world. The United Nations world water development report 2015, p. 12. .
- Urushibara, K. (2012). Karstification processes on minamidaito island in the Nansei Archipelago, Southwest Japan. *Bulletin of the Faculty of Letters, Hosei University*, 65, 83–94. (in Japanese).
- Vacquier, V., Holmes, C. R., Kintzinger, P. R., & Lavergne, M. (1957). Prospecting for ground water by induced electrical polarization. *Geophysics*, 22(3), 660–687.
- Van Genuchten, M. T. (1980). A closed-form equation for predicting the hydraulic conductivity of unsaturated soils. *Soil Science Society of America Journal*, 44(5), 892–898.
- Wen, K. L., Beresnev, I. A., & Yeh, Y. T. (1994). Nonlinear soil amplification inferred from downhole strong seismic motion data. *Geophysical Research Letters*, 21(24), 2625–2628.
- Yang, H., Shimada, J., Matsuda, H., Kagabu, M., & Dong, L. (2015). Evaluation of a freshwater lens configuration using a time series analysis of a groundwater level and an electric conductivity in Minami-daito Island, Okinawa Prefecture Japan. *Journal of Groundwater Hydrology*, 57(2), 187–205.
- Yang, J. (2007). Frequency-dependent amplification of unsaturated surface soil layer. *Journal of Geotechnical and Geoenvironmental Engineering*, 132(4), 526–531.